Molecular Therapy
Nucleic Acids
Original Article

An inflammation-associated lncRNA induces neuronal damage via mitochondrial dysfunction

Ane Olazagoitia-Garmendia,[1,2] Henar Rojas-Márquez,[2,3] Tim Trobisch,[4] Cristina Moreno-Castro,[5] Ariadne Rodriguez Etxebarria,[1] Jon Mentxaka,[1,2] Ajai Tripathi,[6] Bibo Yang,[7] Itziar Martin Ruiz,[8] Juan Anguita,[8,9] J Javier Meana,[2,10,11] Yiliang Ding,[7] Ranjan Dutta,[6] Lucas Schirmer,[4,12,13,14] Mariana Igoillo-Esteve,[5] Izortze Santin,[1,2,15] and Ainara Castellanos-Rubio[2,3,9,15]

[1]Department of Biochemistry and Molecular Biology, University of Basque Country UPV/EHU, 48940 Leioa, Spain; [2]Biobizkaia Health Research Institute, Cruces-Barakaldo 48903, Spain; [3]Department of Genetics, Physical Anthropology and Animal Physiology, University of the Basque Country UPV/EHU, 48940 Leioa, Spain; [4]Department of Neurology, Medical Faculty Mannheim, Heidelberg University, 68167 Mannheim, Germany; [5]ULB Center for Diabetes Research, Université Libre de Bruxelles (ULB), 1050 Bruxelles, Belgium; [6]Department of Neuroscience, Lerner Research Institute, Cleveland Clinic, Cleveland OH 44106, US; [7]Department of Cell and Developmental Biology, John Innes Centre, Norwich Research Park, Norwich NR4 7UH, UK; [8]CIC bioGUNE-BRTA, 48160 Derio, Spain; [9]Ikerbasque, Basque Foundation for Science, 48009 Bilbao, Spain; [10]Department of Pharmacology, University of the Basque Country UPV/EHU, 48940 Leioa, Spain; [11]Centro de Investigación Biomédica en Red de Salud Mental, CIBERSAM, 28029 Madrid, Spain; [12]Mannheim Center for Translational Neuroscience, Medical Faculty Mannheim, Heidelberg University, 68167 Mannheim, Germany; [13]Mannheim Institute for Innate Immunoscience, Medical Faculty Mannheim, Heidelberg University, 68167 Mannheim, Germany; [14]Interdisciplinary Center for Neurosciences, Heidelberg University, 69117 Heidelberg, Germany; [15]CIBERDEM, 28029 Madrid, Spain

Immune disease-associated non-coding SNPs, which often locate in tissue-specific regulatory elements, are emerging as key factors in gene regulation. Among these elements, long non-coding RNAs (lncRNAs) participate in many cellular processes, and their characteristics make these molecules appealing therapeutic targets. In this study, we have studied lncRNA *LOC339803* in the context of neuronal cells, which is located in autoimmunity-associated region 2p15 and recently described to have a proinflammatory role in intestinal disorders. Using human brain samples and a wide variety of *in vitro* techniques, we have showed a differential function of this lncRNA in neuronal cells. We have further demonstrated the role of *LOC339803* in maintaining hexokinase 2 (HK2) levels and thus mitochondrial integrity, partially explaining the implication of the lncRNA in multiple sclerosis (MS) pathogenesis. Our results show the importance of cell-type-specific studies in the case of regulatory lncRNAs. We present *LOC339803* as a candidate for further studies as a mitochondrial dysfunction marker or possible therapeutic target in neurodegeneration.

INTRODUCTION

Over the last few decades, Genome-Wide Association Studies (GWAS) and Immunochip mapping have identified numerous autoimmune disease (AID) loci, providing valuable insights into complex diseases.[1,2] The identification of gene variants implicated in immune disorders has aided not only in risk prediction but also in illuminating some underlying biological mechanisms, thereby opening venues for novel strategies in prevention, diagnosis, and treatment.[3] Nevertheless, the use of genetic evidence in drug discovery remains limited,[4] most probably due to their predominant localization in non-coding genomic regions and their individual small effect size, making it difficult to understand the underlying biological function or the key players associated with these variants.[5,6] However, a recent study has highlighted the importance of the use of genetic evidence in drug discovery and showed that a small genetic effect size is not negatively correlated with clinical success rates. Furthermore, this report highlights the value of studies based on genetic evidence for increased success in drug development.[4]

In the past decade, it has been noted that disease-associated single nucleotide polymorphisms (SNPs) are enriched in long non-coding RNAs (lncRNAs),[7,8] suggesting that they are interesting disease-susceptibility candidate genes. LncRNAs are a varied category of RNA molecules spanning over 200 nucleotides in length that have low or no coding potential and their expression is rather tissue and cell type specific in comparison to that of protein-coding genes.[9] While they have been described to localize in all cell compartments, they

Received 26 August 2024; accepted 31 March 2025;
https://doi.org/10.1016/j.omtn.2025.102533.

Correspondence: Ane Olazagoitia-Garmendia, Department of Biochemistry and Molecular Biology, University of Basque Country UPV/EHU, Leioa 48940, Spain.
E-mail: ane.olazagoitia@ehu.eus
Correspondence: Ainara Castellanos-Rubio, Biobizkaia Health Research Institute, Cruces-Barakaldo 48903, Spain
E-mail: ainara.castellanos@ehu.eus

Published by Elsevier Inc. on behalf of The American Society of Gene and Cell Therapy.
This is an open access article under the CC BY-NC-ND license (http://creativecommons.org/licenses/by-nc-nd/4.0/).

predominantly reside within the nucleus. Thus far, lncRNAs have been linked to virtually every stage of the gene life cycle, including transcription, mRNA splicing, RNA decay, and translation. Indeed, lncRNAs can respond to external stimuli in a quick and cell-type-specific manner, acting both transcriptionally or post-transcriptionally.[7,8,10,11] Moreover, a lncRNA can participate in the pathogenesis of more than one disease, activating specific pathways, which lead to diverse clinical phenotypes.[7,12–14] Hence, deciphering the role of immunity-associated SNPs in lncRNA function may help to understand the pathogenesis of these complex disorders.

AIDs are a clinically heterogeneous group of diseases that affect more than 7% of the population. Genetic and environmental factors have been identified to play a major role in the development of these disorders. Aberrant cytokine responses to environmental triggers produced by immune and non-immune cells, such as epithelial cells, keratinocytes, or neurons, lead to chronic inflammation and destruction of healthy tissues causing a wide range of autoimmune diseases, such as rheumatoid arthritis (RA), lupus, multiple sclerosis (MS), and type 1 diabetes, among others.[3] Although symptomatic therapies may help in some cases, more effective and specific treatments for these diseases are still needed.[15,16] In this line, studying AID-associated SNPs that reside on lncRNAs is a poorly explored but promising approach toward disease-specific successful therapies, as these molecules have shown to be valuable disease-specific biomarkers as well as potential targets for future personalized therapeutic approaches.[17–19]

Starting from an inflammatory-associated SNP, we have recently performed a functional study describing the implication of *LOC339803* lncRNA in the development of intestinal inflammatory disorders. We showed that allele-specific RNA methylation levels affect *LOC339803* function in intestinal cells, facilitating the formation of a chromatin repressor complex in the presence of the more methylated risk allele.[20] Our study demonstrated that increased levels of this lncRNA exacerbate inflammation in the intestine, predisposing to develop intestinal inflammatory disorders and emerging as a potential therapeutic target. The region in which this lncRNA is located is also associated with other immune disorders,[21] such as MS,[22] a chronic AID affecting the central nervous system (CNS), including the brain and spinal cord.[23] MS pathogenesis is still unclear and there is a need of new disease markers and targeted therapies.[24,25] Given the increasing evidence that cell- and tissue-specific expression of lncRNAs provide these molecules the capacity to exert critical functions in the brain,[26,27] we aimed to better understand the implication of *LOC339803* in disease development as well as to elucidate its possible use as a therapeutic target in MS.

Using human brain samples and an *in vitro* neuronal cell line model, we have characterized the involvement of *LOC339803* in mitochondrial integrity in neuronal cells. Our results point to a possible implication of this lncRNA in MS, emerging as a good candidate for future studies finding biomarkers or targeted drugs in MS and stressing the importance of tissue-specific studies of lncRNAs.

RESULTS

Inflammation-associated *LOC339803* in human cortical samples and MS

As mentioned previously, the genomic region where *LOC339803* is located (2q15) is associated with several immune disorders including MS[20,28] (Figure 1A). The MS-associated SNP rs1177228 is located within this region[22] (Figures S1A and S1B), and its reference allele A is correlated with the reference allele A of the SNP rs11498, associated with intestinal inflammation, and located within *LOC339803* lncRNA (Figure S1B). Interestingly, while G genotype increases the risk in intestinal disorders, it is the protective allele for MS (Figure S1C).

We found that *LOC339803* is highly expressed in brain tissue according to different databases[29,30] and RT-qPCR quantification of a commercial RNA pool from diverse human tissues (Figure 1B). Analysis of single cell RNA sequencing (scRNAseq) data from Allen Brain Atlas revealed that the expression of *LOC339803* varies across different brain regions and it is more widely expressed in neuronal than non-neuronal cells from cerebral cortex (Figure 1C). We also quantified *LOC339803* expression by RT-qPCR in human cortical samples and intestinal samples and confirmed the abundant expression of this lncRNA in cortical samples compared to intestinal samples (Figure S1D). Of note, *LOC339803* expression did not vary when sex of individuals was considered (Figure S1E) and showed no correlation with the age of individuals (Spearman r = 0.2355, $p = 0.1732$) in cortical samples (Figure S1F).

Interestingly, when analyzing demyelinated gray matter from MS patients, we observed reduced *LOC339803* levels, both by RT-qPCR (Figure S1G) and RNAscope (Figure 1D). Considering *LOC339803* is more abundant in neuronal cells than in non-neuronal (Figure 1C), our results provide evidence of decreased levels of *LOC339803* in cortical neurons in MS patients. Therefore, we aimed to elucidate the function of *LOC339803* in the neuronal cells.

LOC339803 shows cell-type-specific characteristics

Increased *LOC339803* levels result in a m^6A methylation-dependent reduction of *COMMD1* gene transcription in intestinal cells.[20] We, therefore, wanted to study whether *LOC339803* has the same function in neuronal cells. We first quantified *LOC339803* expression in the human SH-SY5Y neuroblastoma cell line as well as other intestinal and immune cell lines. As observed in human tissues, *LOC339803* was highly expressed in SH-SY5Y cells compared to the rest of cell lines (Figure S2A), suggesting that SH-SY5Y cells are a good model for our studies.

Although *COMMD1* expression is lower in neuronal SH-SY5Y than in intestinal HCT-15 cells (data not shown) the overexpression or silencing of *LOC339803* in SH-SY5Y cells did not affect *COMMD1* transcription (Figures S2B and S2C), indicating that *LOC339803* has a different activity in brain and intestinal tissues. Additionally,

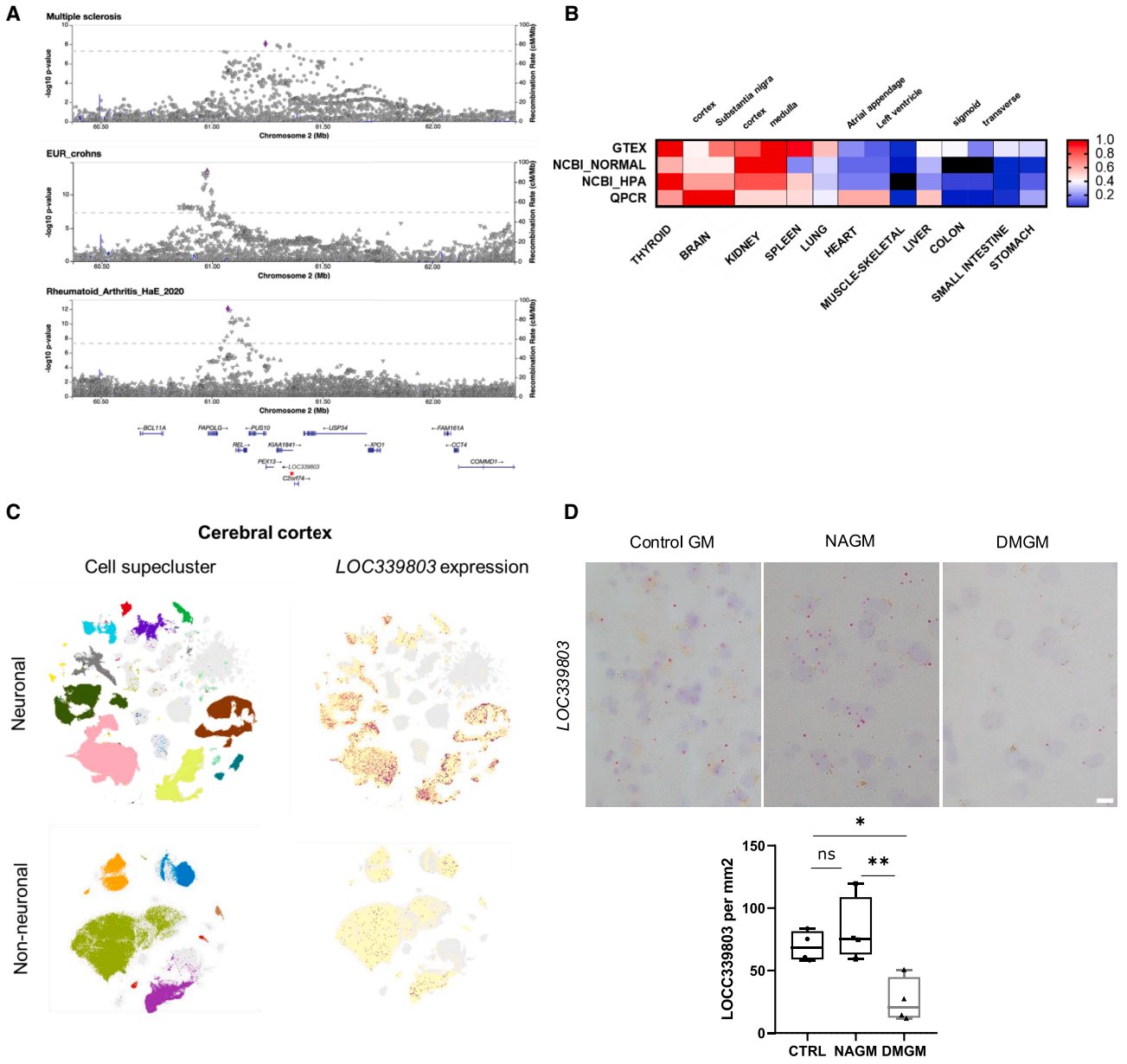

Figure 1. Inflammation-associated *LOC339803* in human cortical samples and MS

(A) Association of 2q15 genomic region in multiple sclerosis, Crohn's disease, and rheumatoid arthritis using LocusZoom. *LOC339803* is highlighted in red. (B) Heatmap graph for *LOC339803* expression in different tissues according to online data (GTEX and NCBI) and RT-qPCR quantification of a commercial RNA pool. (C) scRNAseq data of *LOC339803* in cerebral cortex data according to Allen Brain Atlas. (D) Left, representative images and right quantification of *LOC339803* by RNAscope in control and MS patients ($n = 4$). Scale bars, 20 μm. Data represent the mean and standard error. p values determined by one-way ANOVA test. $^{*}p < 0.05$, $^{**}p < 0.01$, ns = not significant. GM = gray matter; NAGM = normal appearing gray matter; DMGM = demyelinated gray matter.

when analyzing scRNAseq data from Allen Brain Atlas, we could observe that unlike *LOC339803*, *COMMD1* is expressed both in neuronal and non-neuronal cell types at high levels (Figure S2D), showing no apparent correlation with lncRNA expression. Moreover, when m^{6}A methylation status of *LOC339803* was determined, differences between cell lines were also detected. We performed m^{6}A RNA immunoprecipitation (meRIP) in both cell lines and found high levels of methylation of *LOC339803* in HCT-15 intestinal cells, mainly in the LOC G form (Figure 2A, right). However, m^{6}A methylation was barely detectable in SH-SY5Y neuronal cells (Figure 2A, left), suggesting that m^{6}A methylation may not be crucial for its function in this cell type.

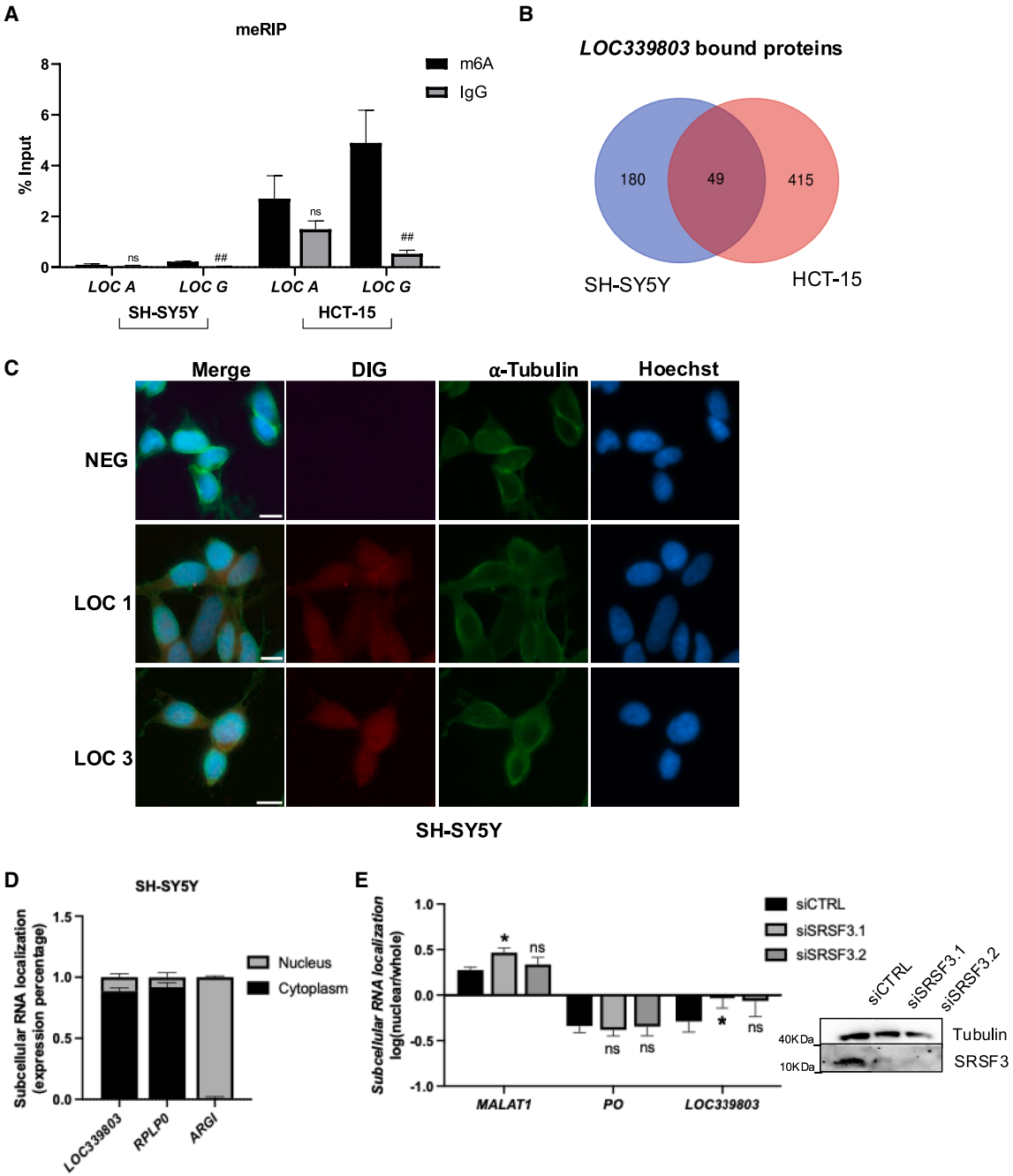

Figure 2. *LOC339803* shows cell-type-specific characteristics

(A) m^{6}A RNA immunoprecipitation (meRIP) and allele-specific *LOC339803* levels (LOC A and LOC G) assessed by RT-qPCR in SH-SY5Y neuronal (n = 3) and HCT-15 intestinal (n = 4) cells. (B) Venn diagram of proteins identified by mass spectrometry in cell-type-specific *LOC339803* IVT pull down. (C) Subcellular localization of *LOC339803* in neuronal SH-SY5Y cell line by fluorescence *in situ* hybridization (FISH). Two different probes with Digoxigenin (DIG) tags (red) were used (LOC1 located in exon1, and LOC3 located in exon2). α-Tubulin (green) was used as cytoplasmic control and Hoechst (blue) as nuclear marker. Scale bars, 10 μm. (D) Subcellular localization of *LOC339803* in SH-SY5Y cell line by biochemical fractionation using RPLP0 and ARGI lncRNA as cytoplasmic and nuclear controls respectively (n = 4). (E) Subcellular localization of *LOC339803* using RPLP0 (cytoplasmic) and MALAT1 (nuclear) as controls upon SRSF3 silencing (n = 3) in SH-SY5Y cells. All p values were determined by two-way ANOVA test. Data represent the mean and standard error *p < 0.05, ns = not significant. Enrichment relative to control IgG ##p < 0.01.

Secondary structure of lncRNAs is usually essential for their mechanism of action, so we next addressed whether m^{6}A methylation and the SNP genotype could be affecting the secondary structure of *LOC339803*, what in turn, could be influencing its cell-type-specific function. With this aim, we analyzed the predicted secondary structure of the lncRNA depending on rs11498 SNP genotype (LOC A or LOC G forms) and m^{6}A motif. We took the advantage of RNA structure ensemble approach because structure ensemble can provide more effective information than single folded structure.[31] Boltzmann sampling of RNA structures was used to sample 1000 structures for both SNP-U (RNA from LOC A form) and SNP-C (RNA from LOC G form) *LOC339803* sequences containing m^{6}A site.[32] Five major groups and representative structures of all the groups were identified after K-means clustering of combined 2000 structures. Cluster 2, 4, and 5 contain SNP-U structures (RNA from LOC A form) as major populations, while 96.4% of structures in cluster 3 belong to SNP-C ensemble (RNA from LOC G form) (Figure S2E). All three SNP-U representative structures show double-strandedness at m^{6}A site and single-strandedness at SNP-U site. In SNP-C representative structure, SNP site is folded with m^{6}A site in single strand region, pointing that this form will be more accessible to be methylated, as we could observe in HCT-15 cells (Figure 2A). These results suggest that both the SNP genotype and m^{6}A methylation could modulate lncRNA structure, and thus, lncRNA function.

Both subcellular localization and protein binding are key characteristics to understand the cellular function of lncRNAs.[33] To further confirm the differential function of *LOC339803* in each cell type, we performed an *in vitro* transcribed (IVT) lncRNA immunoprecipitation followed by mass spectrometry in the SH-SY5Y and HCT-15 cell lines. Although some binding proteins were common in both cell lines, *LOC339803* showed cell-type-specific interacting partners (Figure 2B and Table S1). We also confirmed that, while it is primary nuclear in intestinal cells[20] (Figure S2F), *LOC339803* is widely present in the cytoplasm of neurons, both in the SH-SY5Y cell line (Figures 2C and 2D) and in cortical sections from control individuals (Figure S2G), reinforcing that this lncRNA functions differently in each cell type.

We next aimed to study how *LOC339803* is exported to the cytoplasm in neuronal cells and whether m^{6}A methylation is involved in this process. It has been described that different nuclear export mechanisms are involved in cytoplasmic lncRNA export.[34] The YTHDC1 m^{6}A reader, which interacts with *LOC339803* and regulates the nuclear localization of the lncRNA in intestinal cells,[20] has also been linked with the export mechanism of SRSF3-NXF1.[35] *LOC339803* is a transcript with few and long exons (Figure S1A) and based on previous studies[34] NXF1 silencing influenced its nuclear export (Figure S2H). We analyzed the protein expression and localization of both NXF1 and SRSF3 export proteins in SH-SY5Y and HCT-15 cell lines and showed that the expression levels and subcellular localization are different in each cell line (Figure S2I). Indeed, while SRSF3 is nuclear in HCT-15 cells, it is also present in the cytoplasm of SH-SY5Y cells (Figures S2I and 2J). We next wanted to confirm that these proteins interact with *LOC399803* for its nuclear export in SH-SY5Y cells. Although we could not detect NXF1 enrichment in our IVT RIP in SH-SY5Y cell fraction, we could observe SRSF3 and *LOC339803* interaction by mass spectrometry (Table S1) which was further confirmed by RNA immunoprecipitation (Figure S2K). In addition, silencing of SRSF3 protein resulted in increased nuclear retention of the lncRNA, indicating that the export of *LOC339803* to the neuron cytoplasm is mediated by an NXF1/SRSF3 export complex, being the interaction between *LOC339803* and SRSF3 key for this export (Figure 2E). In accordance with the low m^{6}A methylation levels (Figure 2A) and low YTHDC1 protein expression (Figure S2L) in SH-SY5Y cells; *LOC339803* was shown to contain an m^{6}A independent cytoplasmic localization in neuronal cells, as despite interacting with YTHDC1 (Figure S2M), silencing of the m^{6}A reader YTHDC1 did not influence its cytoplasmic localization (Figure S2N).

Overall, these results suggested that *LOC339803* has a tissue-specific function and while it regulates transcription of *COMMD1* in the nucleus of intestinal cells by an m^{6}A-mediated mechanism, it is exported to the cytoplasm by an m^{6}A independent mechanism in neuronal cells, where it likely participates in other cellular processes.

Cytoplasmic *LOC339803* interacts with metabolic proteins

To further study *LOC339803* cellular function in neuronal cells, we performed an enrichment analysis of the cytoplasmic proteins bound to *LOC339803* in SH-SY5Y cells using ShinyGO. We observed an enrichment of proteins related to ribosome and metabolic pathways (Figures 3A and S3A). We could not confirm interaction between *LOC339803* and ribosomal protein RLP10 by RIP (Figure S3B). Moreover, an *in silico* analysis of coding capacity using Coding Potential Calculator[36] points to a weak coding capacity of *LOC339803* (score: 0.78). Among metabolic proteins, hexokinase 2 (HK2) was of particular interest as it participates in the first step of glycolysis but has also been related to mitochondrial membrane protection,[37] both key processes in neuronal cell metabolism and MS development.[38–41] We confirmed that *LOC339803* binds HK2 protein using RIP (Sup Figure 3C). Moreover, our data showed that this interaction most likely occurs in the cytoplasm, as it is where the majority of the lncRNA is located (Figure 3B).

To better understand the biological implication of the interaction between *LOC339803* and HK2 in neuronal function and MS pathogenesis, we silenced the lncRNA using two different siRNAs (Figure S2C) mimicking what we observed in DMGM human samples (Figure 1D). *LOC339803*-silenced cells had reduced HK2 protein levels (Figure 3C) together with an increase of cytochrome *c* (Cyt C) release (Figure 3D), indicating that its expression is critical to avoid mitochondrial damage.

We then tested the influence of *LOC339803*-associated SNP in the predisposition to MS development. No differences in the subcellular localization of *LOC339803* were detected when comparing the risk (LOC A) and protective (LOC G) SNP forms (Figure S3D). Similarly,

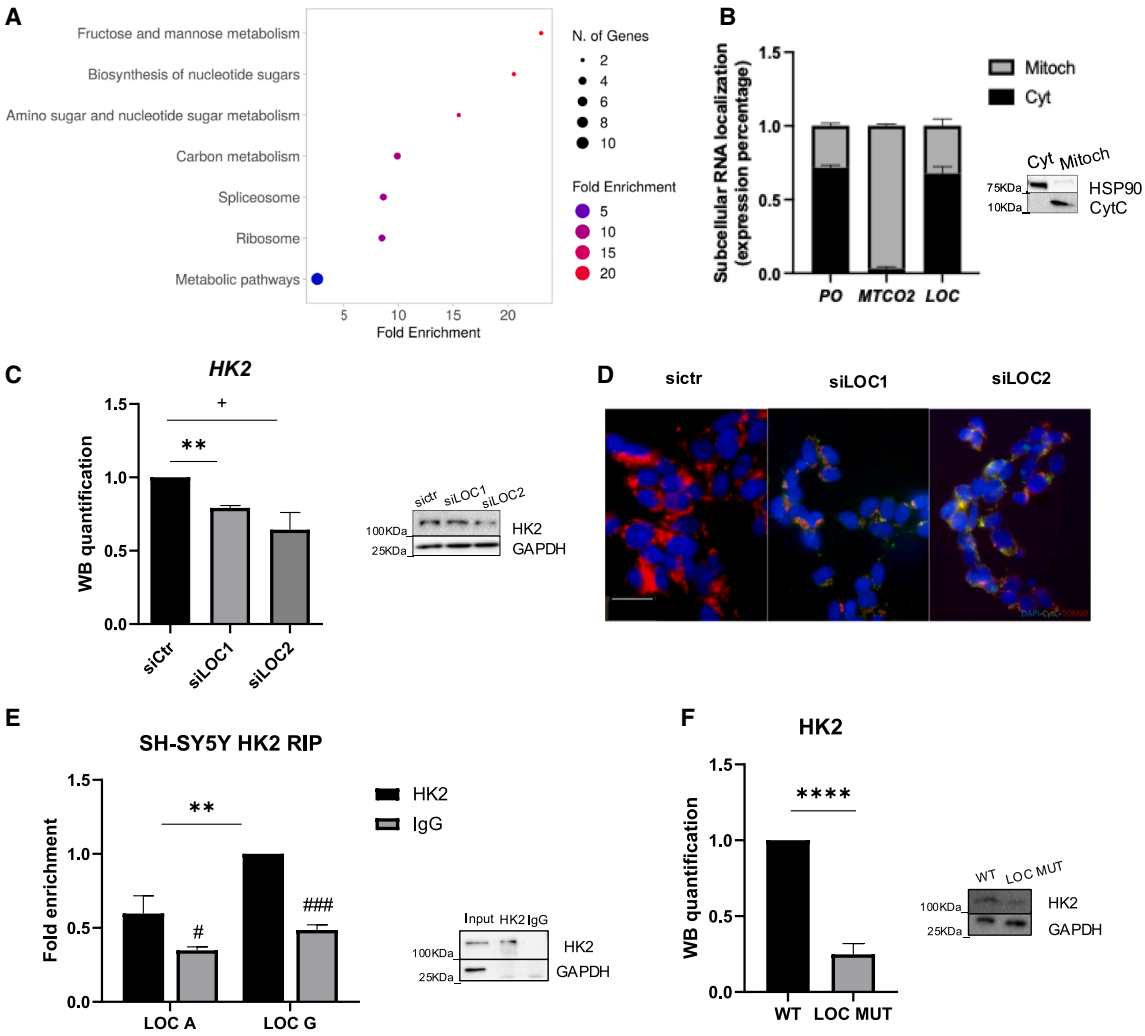

Figure 3. Cytoplasmic *LOC339803* interacts with metabolic proteins

(A) Gene ontology enrichment of cytoplasmic proteins that bind *LOC339803* in SH-SY5Y neuronal cells represented as dotblot chart by ShinyGO, number of genes represented as dot size, and fold enrichment in colors. (B) Subcellular localization of *LOC339803* (LOC) in cytoplasmic and mitochondrial fractions from SH-SY5Y cell line. *RPLP0* (*P0*) and mitochondrial encoded CO2 (*mt-CO2*) were used as cytoplasmic and mitochondrial controls respectively. Data represent the mean and standard error (n = 4). (C) HK2 protein-level quantification and representative immunoblot by western blot in SH-SY5Y cells transfected with control (sictr) or two *LOC339803* targeting siRNA (siLOC1 and siLOC2), GAPDH was used as loading control. Data represent the mean and standard error (n = 4). p values determined by one-way ANOVA test. (D) Co-localization between mitochondria (Tom20, red) and cytochrome *c* (green) in SH-SY5Y cells transfected with control (control) or two *LOC339803* targeting siRNA (siLOC-1 and siLOC-2), nuclei were visualized using DAPI (blue). Scale bars, 20 μm. (E) HK2 immunoprecipitation and quantification of bound allele-specific *LOC339803* (LOC A and LOC G) levels assessed by RT-qPCR in SH-SY5Y neuronal cells. Right, representative immunoblot of the RIP experiment with GAPDH as negative control for the IP. Data represent the mean and standard error (n = 3). p values were determined by two-way ANOVA test. (F) HK2 protein level quantification and representative immunoblot by western blot in SH-SY5Y cells with a mutation of the SNP region in *LOC339803* using CRISPR-Cas9, GAPDH was used as loading control. Data represent the mean and standard error (n = 4). p value determined by unpaired Student's t test. $+p < 0.1$, $^{**}p < 0.01$, $^{****}p < 0.0001$, ns = not significant. Enrichment relative to control IgG $\#p < 0.01$, $\#\#\#p < 0.001$.

the stability of the lncRNA was not affected by the SNP genotype of *LOC339803* (Sup Figure 3E). However, the interaction with HK2 was enhanced by the presence of the protective LOC G form (Figure 3E), indicating the interaction is allele specific. We, therefore, hypothesized that the interaction between the RNA and HK2 occurs within this region. To test this possibility, we performed a CRISPR-Cas9 deletion of the SNP region that disturbed the predicted secondary structure of the RNA (Figure S3F). In these mutant cells, we observed significant reduction of HK2 protein levels (Figure 3F) despite levels of *LOC339803* were unchanged (Figure S3G), showing that the structure of *LOC339803* may be important to maintain proper HK2 protein levels.

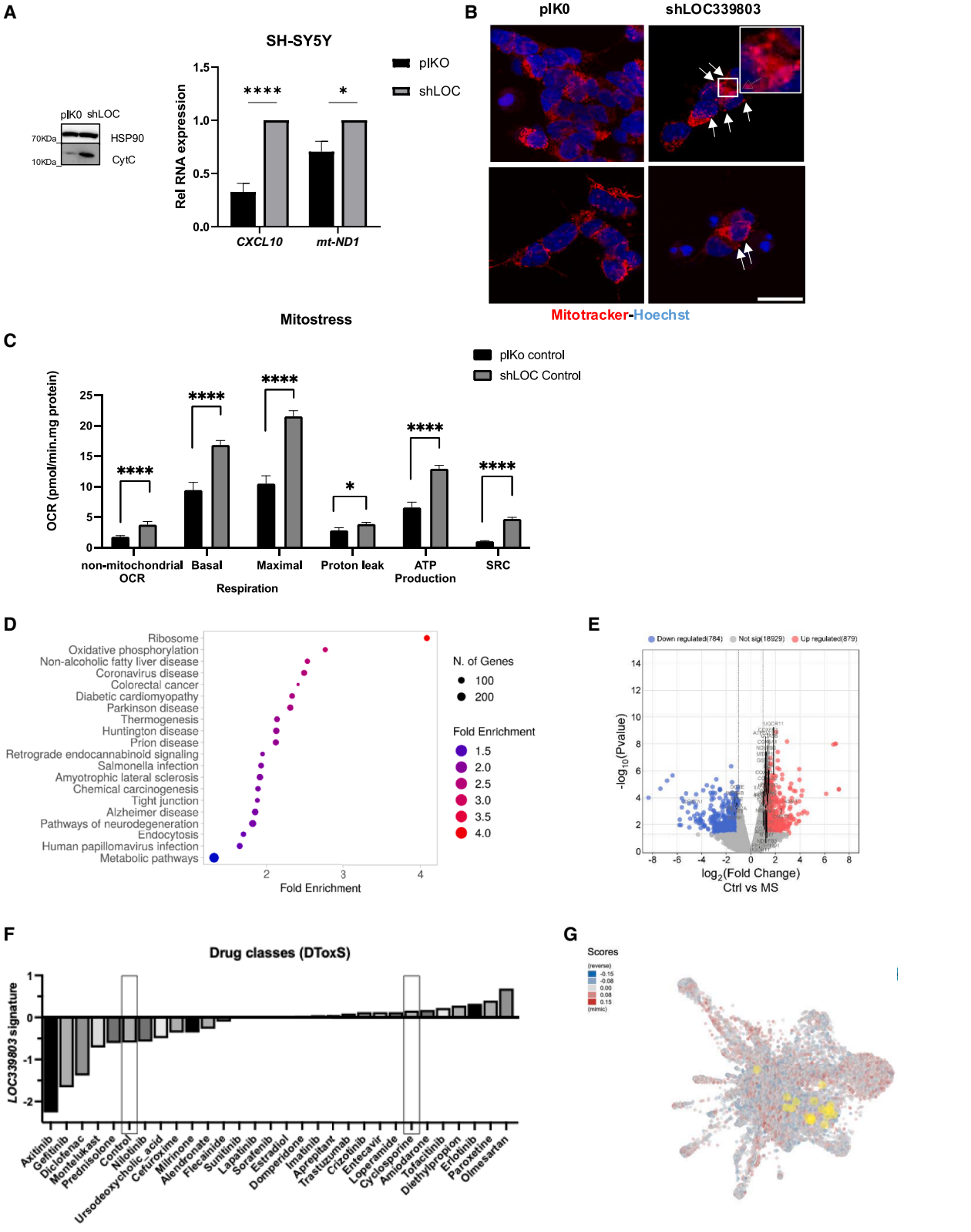

(legend on next page)

Altogether, these results support that *LOC339803* levels, and their secondary structures may be key to maintain HK2 protein amounts and suggest their involvement in mitochondrial protection.

LOC339803 targeting to reverse altered mitochondrial function in MS

Our results show that reduced levels of *LOC339803* lead to lower HK2 protein levels and increased Cyt C release in neuronal cells (sign of mitochondrial membrane disruption) (Figure 3). These results suggest a possible implication of *LOC339803* in mitochondrial damage and altered metabolism characteristic of MS.[39–41] To confirm this, we generated stable *LOC339803* knockdown cells using short hairpin RNAs (Sup Figure 4A). As before (Figure 3D), these cells had augmented Cyt C protein levels (Figures 4A and S4B). Moreover, higher *CXCL10* expression together with increased mitochondrial encoded RNA levels were detected in *LOC339803* silenced cells (Figures 4A and S4C), pointing to a possible activation of the STING pathway and alterations of the mitochondrial activity when *LOC339803* is silenced. The number of mitochondria were not significantly altered in these cells (Sup Figure 1D); nevertheless, we observed increased mitochondria roundness in shLOC339803 cells (Figure 4B), a sign of mitochondrial fission. Moreover, *LOC339803* mutant cells (Figures 3F, S3F, and S3G) also showed increased *CXCL10* proinflammatory cytokine and mitochondrial encoded *ND1* (*mt-ND1*) expression (Figure S4E), again suggesting that the structure of *LOC339803* seems important to maintain mitochondrial integrity.

As HK2 reduction could be influencing both glycolysis and mitochondrial membrane integrity, we performed Seahorse assays to quantify both glycolysis and mitochondrial respiration. No significant changes were detected between plK0 and shLOC cells in their glycolytic capacity (Figure S4F). However, when mitochondrial respiration was assessed, increased non-mitochondrial oxygen consumption rate (OCR), maximal OCR, and proton leak were detected (Figures 4C and S4G), which indicates altered mitochondrial activity and mitochondrial membrane disruption.

These results show that reduced *LOC339803* levels not only affect HK2 protein levels but can also increase mitochondrial membrane disruption. Accumulation of unhealthy mitochondria in cells leads to increased superoxide formation and mitochondrial DNA damage, which would increase risk to MS development. Indeed, pathway enrichment of differentially expressed genes from online available RNAseq data (GSE16461) of relapsing remitting MS (RRMS) patients and control individuals showed a high number of genes participating in metabolic pathways (Figure 4D), being most of them upregulated (Figure 4E). In accordance with our results in MS samples (Figure 1), *LOC339803* expression is also downregulated in RRMS patients compared to controls. Hence, we next overexpressed both *LOC3398903* forms in SH-SY5Y cells to assess if this could reverse disease risk signature. An increase of HK2 protein levels, more significantly with the LOC G form (Figure S4H), which binds HK2 more efficiently (Figure 3E), was observed. Moreover, Cyt C protein levels were also reduced in these cells (Figure S4I). While no specific *LOC339803* targeting small molecules have been described, *LOC339803* signature in different cell lines was analyzed in the DToxS dataset which includes data of FDA approved drugs using iLINCS. The average signature of *LOC339803* in response to each drug was plotted, Olmertasan being the most effective drug on increasing *LOC339803* expression (Figure 4F). Then, the gene signature of RRMS was plotted against L1000 firework display data to identify putative drugs capable to reverse MS signature. Cyclosporine, which we found could induce *LOC33903* expression, showed a significant (p = 3,10-e5) opposite signature to that observed in the MS patients (Figure 4G), suggesting it could reverse the disease phenotype. Additional *in vitro* experiments confirmed that cyclosporine induces *LOC339803* expression in the SH-SY5Y cell line (Figure S4J). What is more, *in vitro* experiments in other cell types showing different degrees of *LOC338903* increase after cyclosporine treatment (Figure S4K) support the ability of this drug to induce *LOC339803* expression.

Collectively, we confirmed that reduced *LOC339803* levels not only affect HK2 protein levels but also lead to mitochondrial damage as represented by higher mitostress values, increased mitochondrial electron transport chain gene expression (as mt-ND1) and mitochondrial roundness. As a result, these cells express more Cyt C and *CXCL10*, which could enhance caspase activation and apoptosis in neuronal cells. Interestingly, cyclosporine, capable of increasing *LOC339803* levels, seems to reverse MS signature, pointing to its possible therapeutic use.

DISCUSSION

This study of lncRNA *LOC339803* in neuronal cells highlights the intricate relationship between RNA molecules, interaction with

Figure 4. *LOC339803* targeting to reverse altered mitochondrial function in MS

(A) Left, quantification of cytochrome *c* protein levels by western blot in control plK0 and *LOC339803* silenced cells using short hairpin RNA silencing (shLOC) in SH-SY5Y neuronal cells, HSP90 was used as loading control. Right, relative RNA quantification of CXCL10 and mt-ND1 by RT-qPCR in plK0 and shLOC. *RPLP0* was used as endogenous control. Data represent the mean and standard error (n = 3). (B) Mitochondrial morphology in control cells (plK0) and *LOC339803* silenced cells (shLOC) using mitotracker and concofal microscopy, nuclei were visualized using Hoechst. Scale bars, 20 μm. (C) Seahorse assay results for OCRs of plK0 control and shLOC cells. Data represent the mean and standard error (n = 5). All p values were determined by two-way ANOVA test. *$p < 0.05$, ****$p < 0.0001$. (D) Gene ontology enrichment of differentially expressed genes from RNAseq data of relapsing-remitting multiple sclerosis (RRMS), control samples represented as dotblot chart by ShinyGO, and number of genes represented as dot size and fold enrichment in colors. (E) Volcano plot of RNAseq data of RRMS and control samples, and genes involved in metabolic pathways are labeled. (F) *LOC339803* expression level upon different drug treatments according to DToxS dataset. (G) Gene signature of RRMS plotted against L1000 firework display data. Yellow dots correspond to cyclosporine signatures.

proteins, and cell type specificity. We found that the function of *LOC339803* varies drastically between neuronal and intestinal cells, indicating a context-dependent role of this lncRNA. While it regulates transcription in intestinal cells, it binds to HK2 protein in the cytoplasm in neuronal cells, modulating its levels and affecting mitochondrial integrity. These results highlight the importance of studying the cell-type-specific lncRNA function using appropriate cell models.

We have observed differences between neuronal and intestinal cells in terms of protein expression and m^6A methylation. Differences in each cell type environment could in turn influence the lncRNA function. For instance, m^6A methylation levels were described to influence the secondary structure of RNA molecules, which is crucial for the ability of lncRNAs to bind their target proteins.[42] We have seen that methylation levels in *LOC339803* are barely detectable in SH-SY5Y cells, while they are abundant in intestinal cells. Therefore, it is plausible to think that the differential methylation levels in each cell type could influence the secondary structure of *LOC339803* and thus affect the cell-type-specific protein binding affinity. Indeed, *LOC339803* binds cell-type-specific proteins, leading to its cytoplasmic localization in neuronal cells while it is located in the nucleus in intestinal cells. Moreover, we could also confirm that the genotype of the SNP could alter the secondary structure of the lncRNA (Figure S2D) what may affect the allele-specific binding of *LOC339803* to HK2 (Figure 3E). All these results highlight the importance of studying context-specific secondary structures of lncRNAs as it could be key to understand their mechanism of action.[42,43]

The interaction between *LOC339803* and HK2 unveils significant implications for mitochondrial function and cellular homeostasis. Apart from its role in glucose phosphorylation, HK2 exhibits the ability to bind to the voltage-dependent anion channel (VDAC) situated on the mitochondrial outer membrane.[37,44] This specific binding facilitates the effective use of ATP generated within the mitochondria as glycolytic fuel, while also serves to stabilize the mitochondrial membrane and to hinder the release of pro-apoptotic factors, including Cyt C.[44] Silencing of *LOC339803* in neuronal cells resulted in reduced HK2 and increased Cyt C release, most probably due to reduced binding of HK2 to mitochondrial membrane. Indeed, disruption of the interaction between HK2 and VDAC could lead to reduction of ATP provision and destabilization of mitochondrial membranes, which could in turn enable mt-DNA release to the cytoplasm and activate STING pathway too.[45] However, it is still unclear what is the mechanism by which *LOC339803* regulates HK2 protein levels.

Mitochondrial dysfunction emerges as a pivotal factor in the pathogenesis of MS, providing new insights into understanding and potentially treating this complex neurological disorder.[39,41,46] Neurons are particularly affected by mitochondrial dysfunction, where in pathological conditions dysregulated mitochondrial dynamics increase negative signals for the cell.[47] We have observed increased expression of mitochondrial electron transport chain mt-ND1 as well as increased mitochondrial respiration in *LOC339803* silenced cells. Mitochondrial dysfunction has been proposed to be prior to neurodegeneration in an experimental autoimmune encephalitis mouse model[48]; hence, mitochondrial alterations caused by downregulation of *LOC339803* could be enhancing neuroinflammation that could later lead to neurodegeneration. Moreover, as a characteristic of mitochondrial membrane disruption due to the reduced binding of HK2 to mitochondria, we also observed increased proton leak levels in *LOC339803* silenced cells. Altogether, these cells presented altered mitochondrial activity, leading to Cyt C release, which can lead to mitochondrial-dependent apoptosis causing neuronal death.[47,49] Interestingly, *CXCL10* proinflammatory cytokine induction was also observed in *LOC339803* silenced cells. Elevated CXCL10 has been correlated with more aggressive disease course[50] while neutralization of this chemokine showed improved neurological function in an animal model.[51] These findings underscore the importance of investigating *LOC339803* involvement in mitochondrial dysfunction in MS and related neurodegenerative diseases. Indeed, overexpression of both *LOC3398903* forms in SH-SY5Y cells resulted in an increase of HK2 protein amounts, and reduced Cyt C protein levels, suggesting that *LOC339803* could be an interesting therapeutic target. What is more, we were able to identify a variety of drugs capable to induce *LOC339803* expression levels. In the case of cyclosporine, apart from inducing *LOC339803* expression in SH-SHY5 cells and other cell types, MS signature was found to be reversed, pointing that targeting *LOC339803* regulated pathways could be a good approach for MS therapy.

In summary, the tissue-specific function of *LOC339803*, coupled with its involvement in mitochondrial dysfunction and neuronal damage, positions it as a promising biomarker and therapeutic target for complex neurological disorders like MS. Moreover, the differential cell-type-specific m^6A methylation of *LOC339803* emphasizes the importance of epigenetic regulation in shaping cellular function. Understanding the role of *LOC339803* in modulating mitochondrial integrity could provide valuable insights into disease mechanisms. Hence, future research aimed at elucidating the precise mechanisms underlying *LOC339803* function and exploring its therapeutic potential holds promise for advancing precision medicine approaches in neurological disorders.

MATERIALS AND METHODS

Experimental model and study participant details

Study participants

For human brain studies, postmortem frontal cortex samples from individuals without neuropsychiatric disorders were obtained at autopsy performed in the Basque Institute of Legal Medicine. Samples were obtained according to Spanish regulations for postmortem studies and were stored in the brain repository of the UPV/EHU (Spain) until assay. Myelinated and demyelinated gray matter samples from progressive MS patients were obtained from Cleveland Clinic, Lerner Research Institute (USA), and from the UK Multiple Sclerosis Tissue Bank at Imperial College, London via prospective

donor scheme following ethical approval by the National Research Ethics Committee in the UK (08/MRE09/31). The use of human samples was approved by the Institutional Review Board of the UPV/EHU (CEIC, E16/46).

Cell lines and treatments

Neuronal SH-SY5Y cell line was purchased from ATCC (#CRL-2266) and cultured in DMEM (Lonza, Basel, Switzerland, #12-604F) supplemented with 10% FBS (Millipore, Burlington, MA, USA, #S0115), 100 units/mL penicillin and 100 μg/mL streptomycin (Lonza, #17-602E). Intestinal HCT-15 (#91030712) cell line was purchased from Sigma-Aldrich (Poole, UK) and cultured in RPMI (Lonza, #12-115F) with 10% FBS, 100 units/mL penicillin and 100 μg/mL streptomycin. U937 (#CRL-3253), THP-1 (#TIB-202) and JURKAT (#TIB-152) cell lines were purchased from ATCC and cultured as suggested by manufacturer.

SH-SY5Y cells were treated with actinomycin D (Sigma-Aldrich, #A9415) at a final concentration of 5 μg/mL for 2 h, 4 h, and 8 h for lncRNA stability assay.

SH-SY5Y cells were treated with cyclosporine (Sigma-Aldrich, #30024) at final concentration of 1 μM for 2 h, 6 h, and 24 h.

Method details

Gene expression analyses

We used 500–1000 ng of RNA for the retrotranscription reaction using iScript cDNA Synthesis Kit (BioRad, CA, USA, #1708890). Expression values were determined by RT-qPCR using Sybr Green (iTaq SYBR Green Supermix, Bio-Rad, #1725124) and specific primers. RPLP0 gene was used as endogenous control in both human samples and cell lines. Reactions were run in a BioRad CFX384 and melting curves were analyzed to ensure the amplification of a single product. All qPCR measurements were performed in duplicates and expression levels were analyzed using the 2–ΔΔCt method and normalization to the highest value was used for relative RNA expression calculation. For *LOC339803* expression analysis, a TaqMan assay with a specific fluorophore for each allele was used when evaluating both alleles at the same time (this could be done because both used cell lines, SH-SY5Y and HCT-15, are heterozygous for rs11498 SNP). For the rest of the experiments, specific primers for the lncRNA and SYBR Green approach were used. All primers are listed in Table S2.

RNAscope

For single-molecule fluorescence *in situ* hybridization (smFISH) validation, we used frozen human cryosections. Staining was performed on representative selection of samples using ACD RNAscope 2.5 HD Red assay. Slides were directly transferred from −80°C into 4% paraformaldehide for fixation: first 15 min at 4°C, and then 2 h at room temperature (RT). After fixation, slides were incubated with H2O2 for 10 min and then boiled in target retrieval solution (ACD) for 5 min. Following a washing step in dH2O slides were dehydrated in 100% EtOH before protease treatment (Protease IV, ACD, 30 min at RT). The target probe (C1) was then incubated on slides for 2 h at 40°C in a specific RNAScope hybridization oven (ACD). The following human RNAScope assay probe was used: C2orf74-DT (C1). Slides were then washed and kept in 5X saline sodium citrate (SSC) overnight. Next day, amplification and probe channel detection steps were performed following manufacturer's recommendation. Slides were then counterstained with 30% hematoxylin for 15 sec and then mounted with Fluoromount reagent (Thermo Fisher Scientific). Brightfield images were taken using a Leica DMi 8 microscope with a Leica DFC7000 GT camera.

FISH

For SH-SY5Y cell line, cells were seeded in 12 mm coverslips and incubated at 37°C. When cells were confluent, the coverslips were transferred to a new 24-well plate with cold 1X PBS and carefully washed by aspirating. Cells were fixed with 4% paraformaldehyde (PFA) and 4% sucrose in 1X PBS for 20 min at 37°C, washed twice with 1X PBS and cold 90% methanol and incubated for 5 min at RT. After washing twice with 1X PBS, cells were blocked with 10% BSA, 0.5% Triton X-100 in 1X PBS buffer, and incubated for 1 h at RT. Cells were then washed three times with 0.5% Triton X-100 in 1X PBS buffer for 10 min each and once with pre-warmed solution 2 (0.1X SSC) for 5 min. 50 μl of the denatured DIG-Probe Mix were spotted on top a Parafilm, coverslips were transferred over the drop (with cells facing the solution) and incubated at 57°C for 60 min in dry oven. Cells were washed with pre-warmed solution 1 (2X SSC, 0.1% Tween 20) and three times with pre-warmed wash solution 2 for 5 min each. The coverslips were incubated with blocking solution (3% BSA, 4xSSC, and 0.1% Tween 20) for 45 min at 37°C in a humid chamber. The primary antibody in a buffer of 0.5% BSA, 0.2% Triton X-100 (TX) in 1X PBS was incubated overnight at 4°C in a humidified chamber. Next day, cells were washed three times with 0.5% Triton X-100 in 1X PBS buffer for 10 min each and incubated in the secondary antibody in a buffer of 0.5% BSA, 0.2% Triton X-100 in 1X PBS for 2 h at RT in the dark (in a humidified chamber). Finally, cells were washed three times with 0.5% Triton X-100 in PBS buffer and three times with 1X PBS for 10 min each. Coverslips were mounted with vectashield, images were taken in an Axio Observer-Zeiss microscope and images were analyzed using the open-software FIJI tool.

For HCT-15 cell line, cells were seeded in 12 mm coverslips and incubated at 37°C. When cells were confluent, they were washed once with 1X PBS at RT and fixed with 4% paraformaldehyde in PBS for 45 min at 4°C. Cells were washed twice with 1X PBS at RT for 5 min and permeabilized with 0.5% Triton X-100 in 1X PBS for 5 min at RT. Cells were washed three times in 1X PBS and once with pre-warmed solution 2 for 5 min each. 50 μl of the denatured DIG-Probe Mix were spotted on top a Parafilm, coverslips were transferred over the drop (with cells facing the solution) and incubated at 57°C for 60 min in dry oven. Cells were washed with pre-warmed solution 1 (2X SSC, 0.1% Tween 20) and three times with pre-warmed wash solution 2 for 5 min each. The coverslips were incubated with blocking solution (3% BSA, 4xSSC, and 0.1%

Tween 20) for 45 min at 37°C in a humid chamber. The primary antibody in a buffer of 3% BSA in 1X PBS was incubated overnight at 4°C in a humidified chamber. Next day, cells were washed three times with 1X PBS buffer for 5 min each and incubated in the secondary antibody in 1X PBS for 1 h at RT in the dark (in a humidified chamber). Finally, cells were washed three times with 1X PBS for 5 min each. Coverslips were mounted with vectashield, images were taken in an Axio Observer-Zeiss microscope, and images were analyzed using the open-software FIJI tool.

m^{6}A RNA immunoprecipitation

We fragmented 4 μg of precleared RNA per sample with RNA fragmentation buffer (100 mM Tris, 2 mM MgCl2) for 3 min at 95°C and placed on ice immediately after heating. 10% of RNA was kept as input; 1 μg of m6A antibody (Abcam, #ab151230) and control antibody (IgG, Santa Cruz Biotechnologies, Dallas, USA, #sc-2025) were coupled to agarose A beads (GE Healthcare, Chicago, USA) in a rotation wheel for 1 h at 4°C. After incubation, beads were washed twice in reaction buffer (150 mM NaCl, 10 mM Tris-HCl, 0.1% NP-40). RNA was added to the antibody-coupled beads and incubated for 3 h at 4°C in a rotating wheel. Subsequently, beads were washed 3X in reaction buffer, 3X in low salt buffer (50 mM NaCl, 10 mM TrisHCl, and 0.1% NP-40) and 3X in high salt buffer (500 mM NaCl, 10 mM TrisHCl, and 0.1% NP-40). After the last wash, beads were resuspended in lysis buffer and RNA was extracted using the PureLink RNA extraction kit (Invitrogen, Carlsbad, USA, #12183016).

RNA immunoprecipitation assay

For SRSF3 RIP experiments, SH-SY5Y cells were lysed in RIP buffer (150 mM KCl, 25 mM Tris, 0.5 mM DTT, 0.5% NP-40, PI), kept on ice for 15 min and homogenized using a syringe. Lysates were precleared with protein A-agarose beads (GE Healthcare, Chicago, USA) for 1 h in a wheel shaker at 4°C. Beads were blocked with 20% BSA and mixed with pre-cleared lysates and 2 μg of anti-IgG antibody (negative control; Santa Cruz Biotechnologies, #sc-2025) or SRSF3 (Santa Cruz Biotechnologies, #sc-13510). After overnight incubation in a wheel shaker at 4°C, beads were washed 3X with RIP buffer, 3X with low salt buffer (50 mM NaCl, 10 mM Tris-HCl, and 0.1% NP-40) and 3X with high salt buffer (500 mM NaCl, 10 mM Tris-HCl, and 0.1% NP-40). After the washes, 70% of beads were resuspended in RNA extraction buffer and 30% was used for western blot (WB).

For HK2, RPL10, and YTHDC1 RIP experiments, SHSY5Y cells were lysed in RIP buffer (150 mM KCl, 25 mM Tris, 0.5 mM DTT, 0.5% NP-40, PI), kept on ice for 15 min and homogenized using a syringe. Lysates were pre-cleared with proteinG dynabeads (Thermo Fisher, Waltman, MA, USA) for 1 h in a wheel shaker at 4°C. Pre-cleared lysates were incubated with 2 μg of anti-IgG antibody or antibody of interest (HK2- Proteintech, #22029-1-AP; RLP10- Proteintech, #17013-1-AP; YTHDC1- Cell Signaling, #E4I9E) for 2 h at RT. After incubation 20 μL dynabeads were added and further incubated for 30 min at RT. The immunoprecipitation was washed three times with RIP buffer, three times with low salt buffer (50 mM NaCl, 10 mM Tris-HCl, 0.1% NP-40) and three times with high salt buffer (500 mM NaCl, 10 mM Tris-HCl, and 0.1% NP-40). After the washes, 70% of beads were resuspended in RNA extraction buffer and 30% was used for WB.

Western blot

Laemmli buffer (62 mM Tris-HCl, 100 mM dithiothreitol (DTT), 10% glycerol, 2% SDS, 0.2 mg/mL bromophenol blue, 5% 2-mercaptoethanol) was added to the protein extracts in radioimmunoprecipitation assay buffer (RIPA) (50 mM Tris HCl, 150 mM NaCl, 1.0% IGEPAL, 0.5% Sodium Deoxycholate, 1.0 mM EDTA, 0.1% SDS, 0.01% sodium azide) and were denatured by heat. Proteins were migrated on 10% SDS-PAGE gels. Following electrophoresis, proteins were transferred onto nitrocellulose membranes using a Transblot-Turbo Transfer System (Biorad) and blocked in 5% non-fatty milk diluted in TBST (20 mM Tris, 150 mM NaCl, and 0.1% Tween 20) at RT for 1 h. The membranes were incubated overnight at 4°C with primary antibodies diluted 1:1000 in TBST. Immunoreactive bands were revealed using the Clarity Max ECL Substrate (BioRad, #1705062) after incubation with a horseradish peroxidase-conjugated anti-mouse or anti-rabbit (1:10000 dilution in 2.5% non-fatty milk) secondary antibody for 1 h at RT. The immunoreactive bands were detected using a Bio-Rad Molecular Imager ChemiDoc XRS and quantified using the ImageJ software. The following antibodies were used for western blotting: YTHDC1 (Abcam, #264375, Cell Signaling, #E4I9E), HK2 (Santa Cruz Biotechnologies, #sc-374091), HSP90 (Cell Signaling; #4874), CYTC (Santa Cruz Biotechnologies, #sc-13156), GAPDH (Santa Cruz Biotechnologies, #sc-47724), SRSF3 (Santa Cruz Biotechnologies, #sc-13510), and ACTIN (Santa Cruz Biotechnologies, #sc47778).

Plasmid construction and overexpression

LOC339803 was amplified from human cDNAs containing A or G allele for rs11498 SNP and cloned into a pCMV6 vector (Origene, #PS100001) using KpnI and FseI restriction sites. The primers used for cloning are listed in Table S2.

For *LOC339803* overexpression, 200 ng of plasmids per 100.000 cells were used. Cells were seeded and transfection was performed with X-TremeGENE HP DNA transfection reagent (Sigma-Aldrich, #6366546001) for 48 h.

Silencing experiments

For *LOC339803*, *SRSF3* or *YTHDC1* silencing, 30 nM of 2 different siRNAs against *LOC339803* (IDT, #hs.Ri.LOC339803.13.1 and hs.Ri.LOC339803.13.2), *SRSF3* (IDT, #hs.Ri.SRSF3.13.2 and hs.Ri.SRSF3.13.3), *YTHDC1* (IDT, #hs.Ri.YTHDC1.13.1 and hs.Ri.YTHDC1.13.3) or negative control siRNA (IDT #51-01-14-01) were transfected into cells using Lipofectamine RNAimax reagent (Invitrogen) for 48 h.

pLKO.1-TRC Cloning vector (Addgene, #10878) was used for the construction of plKO.1-shLOC339803.1 plasmid. Following Addgene's protocol shRNAs were designed to knock down human *LOC339803*. The sequences for the oligos are shown in Table S2. For *LOC339803*

knockdown in SH-SY5Y cell line, viral particles were produced in HEK293FT cells transfected with 1 μg pLKO.1 shRNA plasmid, 750 ng psPAX2 packaging plasmid (Addgene, #12260) and 250 ng pMD2.G envelope plasmid (Addgene, #12259) using X-TremeGENE HP DNA transfection reagent (Sigma-Aldrich, #6366244001) in DMEM without antibiotics and cells were incubated o/n at 37°C. Transfection media was replaced with fresh complete DMEM and viral particle containing media was harvested after 24 h and 48 h. Collected media was centrifuged and concentrated 10 times using Lenti-X concentrator (Takara, #631232). Viral particles were stored in aliquots at −80°C until used. SH-SY5Y cells were infected with sh-LOC339803 or plKO.1 as negative control following Addgene's protocol.

Cellular fractionation

For the quantification of RNA amounts in nuclear and cytoplasmic compartments, nuclei were isolated using C1 lysis buffer (1.28 M sucrose, 40 mM Tris-HCl pH 7.5, 20 mM MgCl2, and 4% Triton X-100). The amounts of LOC339803-A/G, MALAT1 (nuclear control) and RPLP0 (cytoplasmic control) were measured by RT-qPCR and compared to the total amount of those RNAs in the whole cell lysate.

For the quantification of protein amounts in nuclear and cytoplasmic compartments, cells were resuspended in NARA buffer (10 mM HEPES pH 7.9, 10 mM KCl, and 0.1 mM EDTA) with proteinase inhibitors (PI) and incubated in ice for 10 min. After adding NP-40 to final concentration 0.05%, lysates were incubated 5 min in ice and centrifuged at 400 g for 2 min. The supernatant was the cytosolic fraction. Pellet was washed 3X with NARA buffer and resuspended in NARC buffer (20 mM HEPES, 400 mM NaCl, and 1 mM EDTA) + PI, shaken at 4°C for 30 min and centrifuged at 16.000 g for 10 min. The supernatant was the nuclear extract.

For the quantification of RNA and protein amounts in mitochondrial and cytoplasmic compartments, cells were resuspended in MIB buffer (210 mM Mannitol, 70 mM sucrose, 10 mM HEPES pH 7.5, and 1 mM EDTA) + PI and homogenized in ice using a 25-gauge needle fitted on a syringe. After 3 centrifugations at 1500 g for 5 min, all supernatants were collected in ice for further centrifugation at 10000 g for 10 min. Supernatant was cytosolic fraction and pellet the mitochondrial fraction. Mitochondrial fraction was resuspended in 50 μL RIPA+PI and 70% of supernatants were used for RNA extraction and 30% was used for WB.

RNA immunoprecipitation assay followed with mass spectrometry

For RIP-MS experiments, sense and antisense *LOC339803* were amplified from cDNA using a T7 promoter primer. The PCR product was purified and used for *in vitro* transcribing biotinylated RNA using the T7 polymerase (Takara) and RNA biotin labeling kit (Roche). 1 mg of purified *LOC339803* RNA was mixed and incubated with whole cell extracts from HCT-15 and SH-SY5Y cell. Streptavidin beads were added to the reaction and further incubated. After incubation, beads were washed 5 times. Samples were sent for mass spectrometry and subjected to in-solution digestion followed by nano LC-MS/MS analysis. The list of bound proteins was retrieved based on the fold change (sense/antisense). We considered proteins with a fold change higher than 2 as potential interactors of the sense RNA. List of RIP-MS results are shown in Table S1.

Immunofluorescence

For immunostaining of siRNA LOC339803, 1,00,000 SH-SY5Y cells were cultured in μ-slide 8-well high plates (Ibidi, #80806) and washed with PBS 1x after 48 h. Cells were fixed in 4% paraformaldehyde for 10 min and blocked in 0.25% Triton and 3% NGS in PBS1X for 1 h at RT. Samples were incubated with primary antibodies Cyt C (Santa Cruz, #sc-13156) and TOM20 (Abcam, ab186735) (dilution 1:50) overnight at 4°C in a wet chamber. After two washes, the cells were incubated with secondary antibodies at final concentration 1:500 anti-mouse Alexa Fluor 488 (Thermo Fisher Scientific, A-10680) and anti-rabbit Alexa Fluor 594 (Thermo Fisher Scientific, A-11008) respectively for 1 h at RT. Finally, sample were covered with DAPI-mounting medium (Ibidi, #50011) and images were acquired with a confocal microscope (Zeiss LSM800).

To study mitochondrial integrity, 100000 SH-SY5Y cells infected with sh-LOC339803 or plKO.1 were plated in IBIDI plates (#80826) overnight. MitoTracker Orange CM-H2TMRos (Invitrogen, #M7511) was added at 1 mM final concentration for 30 min at 37°C and nuclei were visualized using Hoechst (Sigma-Aldrich, #B2261) at 1.7 μg/mL. Mitochondria were visualized using confocal microscopy (Zeiss LSM880 Airyscan).

Seahorse

Glycolysis and mitochondrial respiration were measured employing an XF24 extracellular flux analyzer (Agilent Technologies), and the measurements were normalized to cellular protein amount.

A mix of 3 different SH-SY5Y cells infected with sh-LOC339803 or plKO.1 were used. 80,000 cells were plated directly in Seahorse plates and incubated in their growth media overnight.

For both OCR and glycolysis determination, the medium of the cells was changed to XF Seahorse medium (Agilent Technologies) supplemented with 4 mM glutamine, 10 mM pyruvate, and 25 mM glucose and were incubated for 1 h at 37°C without CO2.

Then, Mitostress test was performed according to manufacturer's instructions by taking 3 oxigen consumption rate (OCR) and extracellular acidification rate (ECAR) measurements at baseline and after sequentially adding oligomycin (1 μM), FCCP (1 μM), and antimycin/rotenone (0.5 μM)

For glycolytic rate assay 3 measurements are taken at baseline and after sequentially adding antimycin/rotenone (0.5 μM) and 2-DG (50 mM).

Mutant cells generation using CRISPR-Cas9

For mutant cell line generation, two sgRNAs close to the associated SNP were designed and cloned in px458 GFP and px330 mCherry

vectors. SH-SY5Y cells were transfected with 250 ng of each plasmid. Mixed population of the SH-SY5Y cells presenting the expected deletion was used. The sequences for the sgRNAs are shown in Table S1.

LOC339803 *gene expression analysis in online databases*

GTEX and NCBI. Bulk tissue gene expression for *AC016747.3* in thyroid, brain, kidney, spleen, lung, heart, muscle, liver, colon, small intestine, and stomach from GTEX database (https://www.gtexportal.org/home/gene/AC016747.3) was retrieved, and values were normalized to the highest value.

LOC339803 expression from RNA sequencing of total RNA from 20 human tissues and Human Protein Atlas (HPA) RNA-seq normal tissues projects was retrieved from NCBI database (https://www.ncbi.nlm.nih.gov/gene/?term=LOC339803) and values were normalized to the highest value.

Allen brain map. Gene expression of the Human Brain Atlas (https://human.brain-map.org) was used to assess the expression of *LOC339803* in the different brain structures. Allen Brain Cell Atlas (https://knowledge.brain-map.org/abcatlas) was used to visualize the expression of LOC339803 in neuronal and non-neuronal cell.

DToxS and L1000FWD. For the selection of drugs that could induce *LOC339803*, we used DToxS database (https://iyengarlab.org/dtoxs/). We plotted the mean expression of *LOC339803* in different human cell lines after exposure to FDA approved drugs. The drugs that presented induction of the lncRNA were checked in L1000FWD (https://maayanlab.cloud/l1000fwd/) to evaluate their ability to revert MS related gene signature.

Pathway enrichment and protein association analysis

First, we performed a cellular component analysis using gene ontology resource[52–54] selecting the proteins that were enriched only in SH-SY5Y cells according to our IVT-RIP MS results (Table S1). Then, only the cytoplasmic proteins were selected to perform a pathway enrichment using ShinyGo 0.80 KEGG pathway enrichment analysis (FDR cutoff: 0.1).[55]

The STRING database (https://string-db.org/) was used to analyze the protein association networks (both physical and functional interactions) of the cytoplasmic proteins that interact with *LOC339803* and were enriched according to ShinyGo KEGG pathway enrichment.

For the analysis of gene ontology in RNAseq data from RRMS patients and controls (GSE16461), pathway enrichment was performed using ShinyGo 0.80 KEGG pathway enrichment analysis (FDR cutoff: 0.05).

Quantification and statistical analyses

All the statistical analyses were performed using GraphPad Prism 8 (GraphPad Software). Significance was calculated using Student's t test, Mann-Whitney test or ANOVA test as specified in figure legends. The statistically significance level was set at $p < 0.05$. p values lower than 0.1 are marked with a + sign.

Limitations of the study

One limitation of this work is the small amount of human brain samples studied. Opposite to intestinal biopsies that can be acquired with routine endoscopy or colonoscopy techniques, brain samples are collected postmortem, reducing the access to the samples. Therefore, the use of available databases has been helpful to confirm our results in bigger sample sets. Additionally, one of the main drawbacks of our work, that also applies to many others studying lncRNAs,[56] is the lack of a murine homolog for *LOC339803*, making it complicated to perform preclinical studies in murine disease models.

DATA AVAILABILITY

- Plasmids generated in this study are available upon request.
- Data and code used in this study are available upon request.

ACKNOWLEDGMENTS

The authors thank the Analytical and High-Resolution Microscopy in Biomedicine Service of the UPV/EHU SGIker (UPV/EHU/ERDF, EU) for technical and human support provided. This work was supported by grants PID2022-141124NB-I00 funded by the Ministry of Science, Innovation and Universities and grants 2023111056 and IT1739-22 funded by the Basque Government to A.C.-R., grant PID2019-104475GA-I00 funded by MCIN/AEI/10.13039/501100011033 to I.S., grant PID2021-124328B-100 to J.A., grant IT-1512/22 from the Basque Government to J.J.M., Actions de Reserche Concertees de la Communaute Francaise (ARC) to M.I.-E., post-doctoral grant ESPDOC21/56 by UPV/EHU and post-doctoral grant POS_2024_1_0045 by Basque Government to A. O.-G., and predoctoral grant from the Spanish Ministry of Science, Universities and Innovation (PRE2019-089350) to H.R.-M.

AUTHOR CONTRIBUTIONS

A.C.-R. and A.O.-G designed the research. A.O.-G., H.R.-M., T.T., C.M.-C., A.R.E., J.M., A.T., and I.M.R. carried out experiments. J.A., M.I.-E., and I.S. provided technical assistance. J.J.M., R.D., and L.S. collected the clinical samples. B.Y. and Y.D. performed secondary structure analyses. A.C.-R. and A.O.-G. analyzed the data. A.C.-R. and A.O.-G. wrote the manuscript with input from the other authors. All authors read and approved the final manuscript.

DECLARATION OF INTERESTS

The authors declare no competing interests.

SUPPLEMENTAL INFORMATION

Supplemental information can be found online at https://doi.org/10.1016/j.omtn.2025.102533.

REFERENCES

1. Ricaño-Ponce, I., Zhernakova, D.V., Deelen, P., Luo, O., Li, X., Isaacs, A., Karjalainen, J., Di Tommaso, J., Borek, Z.A., Zorro, M.M., et al. (2016). Refined mapping of autoimmune disease associated genetic variants with gene expression suggests an important role for non-coding RNAs. J. Autoimmun. *68*, 62–74. https://doi.org/10.1016/j.jaut.2016.01.002.

2. Jonkers, I.H., and Wijmenga, C. (2017). Context-specific effects of genetic variants associated with autoimmune disease. Hum Mol Genet *26*, R185. https://doi.org/10.1093/hmg/ddx254.

3. Gutierrez-Arcelus, M., Rich, S.S., and Raychaudhuri, S. (2016). Autoimmune diseases-connecting risk alleles with molecular traits of the immune system. Nat. Rev. Genet. *17*, 160. https://doi.org/10.1038/nrg.2015.33.

4. Minikel, E.V., Painter, J.L., Dong, C.C., and Nelson, M.R. (2024). Refining the impact of genetic evidence on clinical success. Nature *629*, 624–629. https://doi.org/10.1038/s41586-024-07316-0.

5. Tak, Y.G., and Farnham, P.J. (2015). Making sense of GWAS: using epigenomics and genome engineering to understand the functional relevance of SNPs in non-coding regions of the human genome. Epigenetics Chromatin *8*, 1–18. https://doi.org/10.1186/S13072-015-0050-4.

6. Farh, K.K.H., Marson, A., Zhu, J., Kleinewietfeld, M., Housley, W.J., Beik, S., Shoresh, N., Whitton, H., Ryan, R.J.H., Shishkin, A.A., et al. (2014). Genetic and epigenetic fine mapping of causal autoimmune disease variants. Nature *518*, 337–343. https://doi.org/10.1038/nature13835.

7. Castellanos-Rubio, A., and Ghosh, S. (2019). Disease-associated SNPs in inflammation-related lncRNAs. Front. Immunol. *10*, 420–429. https://doi.org/10.3389/fimmu.2019.00420.

8. Mowel, W.K., Kotzin, J.J., McCright, S.J., Neal, V.D., and Henao-Mejia, J. (2018). Control of Immune Cell Homeostasis and Function by lncRNAs (Preprint at Elsevier Ltd). https://doi.org/10.1016/j.it.2017.08.009.

9. Arunkumar, G. (2024). LncRNAs: the good, the bad, and the unknown. Biochem. Cell. Biol. *102*, 9–27. https://doi.org/10.1139/bcb-2023-0155.

10. de Haas, E.C., Kumar, V., and Wijmenga, C. (2014). Immunogenetics of Celiac Disease. In, pp. 53–66. https://doi.org/10.1007/978-1-4614-8560-5_5.

11. Robinson, E.K., Covarrubias, S., and Carpenter, S. (2020). The how and why of lncRNA function: An innate immune perspective. Biochim Biophys Acta Gene Regul Mech *1863*, 194419.

12. Pandini, C., Garofalo, M., Rey, F., Garau, J., Zucca, S., Sproviero, D., Bordoni, M., Berzero, G., Davin, A., Poloni, T.E., et al. (2021). MINCR: A long non-coding RNA shared between cancer and neurodegeneration. Genomics *113*, 4039–4051. https://doi.org/10.1016/j.ygeno.2021.10.008.

13. Castellanos-Rubio, A., Fernandez-Jimenez, N., Kratchmarov, R., Luo, X., Bhagat, G., Green, P.H.R., Schneider, R., Kiledjian, M., Bilbao, J.R., and Ghosh, S. (2016). A long noncoding RNA associated with susceptibility to celiac disease. Science *352*, 91–95. https://doi.org/10.1126/science.aad0467.

14. Gonzalez-Moro, I., Olazagoitia-Garmendia, A., Colli, M.L., Cobo-Vuilleumier, N., Postler, T.S., Marselli, L., Marchetti, P., Ghosh, S., Gauthier, B.R., Eizirik, D.L., et al. (2020). The T1D-associated lncRNA Lnc13 modulates human pancreatic β cell inflammation by allele-specific stabilization of STAT1 mRNA. Proc. Natl. Acad. Sci. USA *117*, 9022–9031. https://doi.org/10.1073/pnas.1914353117.

15. Shandil, R.K., Dhup, S., and Narayanan, S. (2022). Evaluation of the Therapeutic Potential of Mesenchymal Stem Cells (MSCs) in Preclinical Models of Autoimmune Diseases. Stem Cells Int. *2022*, 6379161. https://doi.org/10.1155/2022/6379161.

16. Rosenblum, M.D., Gratz, I.K., Paw, J.S., and Abbas, A.K. (2012). Treating human autoimmunity: Current practice and future prospects. Sci. Transl. Med. *4*, 125sr1. https://doi.org/10.1126/scitranslmed.3003504.

17. Statello, L., Guo, C.J., Chen, L.L., and Huarte, M. (2020). Gene regulation by long non-coding RNAs and its biological functions. Nat. Rev. Mol. Cell Biol. *22*, 96–118. https://doi.org/10.1038/s41580-020-00315-9.

18. Xu, K., Jiang, X., Ariston Gabriel, A.N., Li, X., Wang, Y., and Xu, S. (2021). Evolving Landscape of Long Non-coding RNAs in Cerebrospinal Fluid: A Key Role From Diagnosis to Therapy in Brain Tumors. Front. Cell Dev. Biol. *9*, 737670. https://doi.org/10.3389/FCELL.2021.737670.

19. Katsushima, K., Jallo, G., Eberhart, C.G., and Perera, R.J. (2021). Long non-coding RNAs in brain tumors. NAR Cancer *3*. zcaa041-16. https://doi.org/10.1093/NARCAN/ZCAA041.

20. Olazagoitia-Garmendia, A., Rojas-Márquez, H., Sebastian-delaCruz, M., Agirre-Lizaso, A., Ochoa, A., Mendoza-Gomez, L.M., Perugorria, M.J., Bujanda, L., Madrigal, A.H., Santin, I., et al. (2024). m6A Methylated Long Noncoding RNA LOC339803 Regulates Intestinal Inflammatory Response. Adv. Sci. *11*, e2307928. https://doi.org/10.1002/ADVS.202307928.

21. Lettre, G., and Rioux, J.D. (2008). Autoimmune diseases: insights from genome-wide association studies. Hum. Mol. Genet. *17*, R116–R121. https://doi.org/10.1093/hmg/ddn246.

22. Patsopoulos, N.A., Baranzini, S.E., Santaniello, A., Shoostari, P., Cotsapas, C., Wong, G., Beecham, A.H., James, T., Replogle, J., Vlachos, I.S., et al. (2019). Multiple sclerosis genomic map implicates peripheral immune cells and microglia in susceptibility. Science *365*, AAV7188. https://doi.org/10.1126/SCIENCE.AAV7188.

23. Barkhane, Z., Elmadi, J., Kumar, L.S., Sree Pugalenthi, L., Ahmad, M., and Reddy, S. (2022). Multiple Sclerosis and Autoimmunity: A Veiled Relationship. Bicol Christian College of Medicine, Legazpi *14*, e24294. https://doi.org/10.7759/cureus.24294.

24. Afrasiabi, A., Ahlenstiel, C., Swaminathan, S., and Parnell, G.P. (2023). The interaction between Epstein-Barr virus and multiple sclerosis genetic risk loci: insights into disease pathogenesis and therapeutic opportunities. Clin. Transl. Immunology *12*, e1454. https://doi.org/10.1002/cti2.1454.

25. Ghasemi, N., Razavi, S., and Nikzad, E. (2017). Multiple Sclerosis: Pathogenesis, Symptoms, Diagnoses and Cell-Based Therapy. CELL JOURNAL(Yakhteh) *19*, 1–10.

26. Clark, B.S., and Blackshaw, S. (2017). Understanding the Role of lncRNAs in Nervous System Development. Adv. Exp. Med. Biol. *1008*, 253–282. https://doi.org/10.1007/978-981-10-5203-3_9.

27. Srinivas, T., Mathias, C., Oliveira-Mateos, C., and Guil, S. (2023). Roles of lncRNAs in brain development and pathogenesis: Emerging therapeutic opportunities. Mol. Ther. *31*, 1550–1561. https://doi.org/10.1016/j.ymthe.2023.02.008.

28. Ghoussaini, M., Mountjoy, E., Carmona, M., Peat, G., Schmidt, E.M., Hercules, A., Fumis, L., Miranda, A., Carvalho-Silva, D., Buniello, A., et al. (2021). Open Targets Genetics: systematic identification of trait-associated genes using large-scale genetics and functional genomics. Nucleic Acids Res. *49*, D1311–D1320. https://doi.org/10.1093/nar/gkaa840.

29. GTEx Project (2017). GTEx portal. Preprint. https://www.gtexportal.org/home/gene/AC016747.3.

30. Sayers, E.W., Bolton, E.E., Brister, J.R., Canese, K., Chan, J., Comeau, D.C., Connor, R., Funk, K., Kelly, C., Kim, S., et al. (2022). Database resources of the national center for biotechnology information. Nucleic Acids Res. *50*, D20–D26. https://doi.org/10.1093/NAR/GKAB1112.

31. Kumar, J., Lackey, L., Waldern, J.M., Dey, A., Mustoe, A.M., Weeks, K.M., Mathews, D.H., and Laederach, A. (2022). Quantitative prediction of variant effects on alternative splicing in MAPT using endogenous pre-messenger RNA structure probing. Elife *11*, e73888. https://doi.org/10.7554/ELIFE.73888.

32. Reuter, J.S., and Mathews, D.H. (2010). RNAstructure: Software for RNA secondary structure prediction and analysis. BMC Bioinf. *11*, 129. https://doi.org/10.1186/1471-2105-11-129/FIGURES/3.

33. Bridges, M.C., Daulagala, A.C., and Kourtidis, A. (2021). LNCcation: lncRNA localization and function. J. Cell Biol. *220*, e202009045. https://doi.org/10.1083/JCB.202009045/211695.

34. Zuckerman, B., Ron, M., Mikl, M., Segal, E., and Ulitsky, I. (2020). Gene Architecture and Sequence Composition Underpin Selective Dependency of Nuclear Export of Long RNAs on NXF1 and the TREX Complex. Mol. Cell *79*, 251–267.e6. https://doi.org/10.1016/J.MOLCEL.2020.05.013.

35. Roundtree, I.A., Luo, G.Z., Zhang, Z., Wang, X., Zhou, T., Cui, Y., Sha, J., Huang, X., Guerrero, L., Xie, P., et al. (2017). YTHDC1 mediates nuclear export of N6-methyladenosine methylated mRNAs. Elife *6*, e31311. https://doi.org/10.7554/eLife.31311.

36. Kang, Y.J., Yang, D.C., Kong, L., Hou, M., Meng, Y.Q., Wei, L., and Gao, G. (2017). CPC2: A fast and accurate coding potential calculator based on sequence intrinsic features. Nucleic Acids Res. *45*, W12–W16. https://doi.org/10.1093/nar/gkx428.

37. Wang, Z., Wang, N., Chen, J., and Shen, J. (2012). Emerging glycolysis targeting and drug discovery from Chinese medicine in cancer therapy. Evid. Based. Complement. Alternat. Med. *2012*, 873175. https://doi.org/10.1155/2012/873175.

38. Ghirotto, B., Oliveira, D.F., Cipelli, M., Basso, P.J., De Lima, J., Breda, C.N.S., Ribeiro, H.C., Silva, C.C.C., Sertié, A.L., Oliveira, A.E.R., et al. (2022). MS-Driven Metabolic Alterations Are Recapitulated in iPSC-Derived Astrocytes. Ann. Neurol. *91*, 652–669. https://doi.org/10.1002/ana.26336.

39. Mahad, D., Ziabreva, I., Lassmann, H., and Turnbull, D. (2008). Mitochondrial defects in acute multiple sclerosis lesions. Brain *131*, 1722–1735. https://doi.org/10.1093/brain/awn105.

40. Nijland, P.G., Molenaar, R.J., Van Der Pol, S.M.A., Van Der Valk, P., Van Noorden, C.J.F., De Vries, H.E., and Van Horssen, J. (2015). Differential expression of glucose-metabolizing enzymes in multiple sclerosis lesions. Acta Neuropathol. Commun. *3*, 79. https://doi.org/10.1186/s40478-015-0261-8.

41. Wang, P.F., Jiang, F., Zeng, Q.M., Yin, W.F., Hu, Y.Z., Li, Q., and Hu, Z.L. (2024). Mitochondrial and metabolic dysfunction of peripheral immune cells in multiple sclerosis. J. Neuroinflammation *21*, 28. https://doi.org/10.1186/S12974-024-03016-8.

42. Wang, Y., Traugot, C.M., Bubenik, J.L., Li, T., Sheng, P., Hiers, N.M., Fernandez, P., Li, L., Bian, J., Swanson, M.S., and Xie, M. (2023). N6-methyladenosine in 7SK small nuclear RNA underlies RNA polymerase II transcription regulation. Mol. Cell *83*, 3818–3834.e7. https://doi.org/10.1016/J.MOLCEL.2023.09.020.

43. Frank, F., Kavousi, N., Bountali, A., Dammer, E.B., Mourtada-Maarabouni, M., and Ortlund, E.A. (2020). The lncRNA Growth Arrest Specific 5 Regulates Cell Survival via Distinct Structural Modules with Independent Functions. Cell Rep. *32*, 107933. https://doi.org/10.1016/j.celrep.2020.107933.

44. Pastorino, J.G., and Hoek, J.B. (2008). Regulation of hexokinase binding to VDAC. J. Bioenerg. Biomembr. *40*, 171–182. https://doi.org/10.1007/S10863-008-9148-8.

45. Kim, J., Gupta, R., Blanco, L.P., Yang, S., Shteinfer-Kuzmine, A., Wang, K., Zhu, J., Yoon, H.E., Wang, X., Kerkhofs, M., et al. (2019). VDAC oligomers form mitochondrial pores to release mtDNA fragments and promote lupus-like disease. Science *366*, 1531–1536. https://doi.org/10.1126/SCIENCE.AAV4011.

46. Picone, P., and Nuzzo, D. (2022). Promising Treatment for Multiple Sclerosis: Mitochondrial Transplantation. Int. J. Mol. Sci. *23*, 2245. https://doi.org/10.3390/ijms23042245.

47. Blagov, A.V., Sukhorukov, V.N., Orekhov, A.N., Sazonova, M.A., and Melnichenko, A.A. (2022). Significance of Mitochondrial Dysfunction in the Progression of Multiple Sclerosis. Int. J. Mol. Sci. *23*, 12725. https://doi.org/10.3390/IJMS232112725.

48. Sadeghian, M., Mastrolia, V., Haddad, A.R., Mosley, A., Mullali, G., Schiza, D., Sajic, M., Hargreaves, I., Heales, S., Duchen, M.R., et al. (2016). Mitochondrial Dysfunction Is an Important Cause of Neurological Deficits in an Inflammatory Model of Multiple Sclerosis (Nature Publishing Group). https://doi.org/10.1038/srep33249.

49. Sui, Y., Stehno-Bittel, L., Li, S., Loganathan, R., Dhillon, N.K., Pinson, D., Nath, A., Kolson, D., Narayan, O., and Buch, S. (2006). CXCL10-induced cell death in neurons: role of calcium dysregulation. Eur. J. Neurosci. *23*, 957–964. https://doi.org/10.1111/J.1460-9568.2006.04631.X.

50. Welsh, N., Disano, K., Linzey, M., Pike, S.C., Smith, A.D., Pachner, A.R., and Gilli, F. (2024). CXCL10/IgG1 Axis in Multiple Sclerosis as a Potential Predictive Biomarker of Disease Activity. Neurol. Neuroimmunol. Neuroinflamm. *11*, 200200. https://doi.org/10.1212/NXI.0000000000200200.

51. Liu, M.T., Keirstead, H.S., and Lane, T.E. (2001). Neutralization of the Chemokine CXCL10 Reduces Inflammatory Cell Invasion and Demyelination and Improves Neurological Function in a Viral Model of Multiple Sclerosis 1. J. Immunol. *167*, 4091–4097.

52. Ashburner, M., Ball, C.A., Blake, J.A., Botstein, D., Butler, H., Cherry, J.M., Davis, A. P., Dolinski, K., Dwight, S.S., Eppig, J.T., et al. (2000). Gene ontology: Tool for the unification of biology. Nat. Genet. *25*, 25. https://doi.org/10.1038/75556.

53. Gene Ontology Consortium, Aleksander, S.A., Balhoff, J., Carbon, S., Cherry, J.M., Drabkin, H.J., Ebert, D., Feuermann, M., Gaudet, P., Harris, N.L., and Hill, D.P. (2023). The Gene Ontology knowledgebase in 2023. Genetics *224*, iyad031. https://doi.org/10.1093/GENETICS/IYAD031.

54. Thomas, P.D., Ebert, D., Muruganujan, A., Mushayahama, T., Albou, L.P., and Mi, H. (2022). PANTHER: Making genome-scale phylogenetics accessible to all. Protein Sci. *31*, 8–22. https://doi.org/10.1002/PRO.4218.

55. Ge, S.X., Jung, D., Yao, R., and Yao, R. (2020). ShinyGO: a graphical gene-set enrichment tool for animals and plants. Bioinformatics *36*, 2628–2629. https://doi.org/10.1093/BIOINFORMATICS/BTZ931.

56. Ulitsky, I., Shkumatava, A., Jan, C.H., Sive, H., and Bartel, D.P. (2011). Conserved function of lincRNAs in vertebrate embryonic development despite rapid sequence evolution. Cell *147*, 1537–1550. https://doi.org/10.1016/j.cell.2011.11.055.